

Bow shock's geometry at the magnetospheric flanks

J. Merka

L-3 Communications Government Services, Inc., Vienna, Virginia, USA

A. Szabo

Laboratory for Extraterrestrial Physics, NASA Goddard Space Flight Center, Greenbelt, Maryland, USA

Received 28 April 2004; revised 15 September 2004; accepted 13 October 2004; published 28 December 2004.

[1] The database of IMP 8 bow shock crossings was used to investigate properties of the bow shock's cross section between 10 and 15 R_E tailward of Earth in response to selected upstream and magnetospheric parameters. Best-fitted ellipses were derived for each parameter subset and analyzed. We have found that for average solar wind conditions, the shock's cross section moves in the north-south directions by 3.8 R_E when the dipole tilt changes from sunward to antisunward orientations. Comparisons with results provided by global three-dimensional MHD simulations of the magnetosphere have shown that the tilt angle effect is likely to be also important for the estimation of the dayside shock wave's position. We have found the orientation of the IMF with respect to the solar wind flow, expressed by the angle θ_{BV} , to influence the size and stability of the shock shape/position. The observed Mach number dependence agreed with previous studies and no other significant IMF-induced asymmetries were found. *INDEX TERMS:* 2154

Interplanetary Physics: Planetary bow shocks; 2784 Magnetospheric Physics: Solar wind/magnetosphere interactions; 7851 Space Plasma Physics: Shock waves; 2724 Magnetospheric Physics: Magnetopause, cusp, and boundary layers; *KEYWORDS:* terrestrial bow shock, magnetopause, solar wind-magnetosphere interaction, IMP 8, dipole tilt angle

Citation: Merka, J., and A. Szabo (2004), Bow shock's geometry at the magnetospheric flanks, *J. Geophys. Res.*, 109, A12224, doi:10.1029/2004JA010567.

1. Introduction

[2] The interaction of supersonic magnetized solar wind plasma with the Earth's magnetic field forms the magnetosphere and a fast magnetosonic wave, the bow shock. The boundary layer between the magnetosphere and the shocked solar wind (plasma downstream of the shock) is called the magnetopause. The configuration of both the magnetopause and the bow shock is very dynamic and depends on both the solar wind and magnetospheric properties. In addition to the solar wind influence, the shape and size of the magnetopause depends on the Earth's magnetic field.

[3] The existence of a magnetospheric boundary, the magnetopause, was first proposed by *Chapman and Ferraro* [1931]. They also proposed that solar wind dynamic pressure p_{sw} controls the location of the magnetopause. In the gasdynamic approximation, a balance between the magnetic pressure of the Earth's magnetic field and the solar wind dynamic pressure defines the location of the magnetopause [see *Spreiter et al.*, 1966, and references therein]. The magnetospheric magnetic field is nearly constant, at least in the gasdynamic approximation, but the dynamic pressure can change significantly and suddenly. Thus the magnetopause standoff distance decreases when dynamic pressure increases and vice versa.

[4] *Aubry et al.* [1970] suggested that erosion of magnetic flux from the dayside magnetosphere to the tail also results in an inward motion of the magnetopause during southward IMF orientation. The *Fairfield* [1971] study confirmed this suggestion and showed that more earthward crossings are associated with larger southward IMF.

[5] Many magnetopause models have been developed for various ram pressure and/or IMF B_z conditions [e.g., *Fairfield*, 1971; *Holzer and Slavin*, 1978; *Formisano et al.*, 1979; *Sibeck et al.*, 1991; *Petrinec et al.*, 1991; *Petrinec and Russell*, 1993, 1996; *Roelof and Sibeck*, 1993; *Shue et al.*, 1997, 1998; *Kuznetsov and Suvorova*, 1998; *Kawano et al.*, 1999; *Dmitriev and Suvorova*, 2000]. The shape of the magnetopause is often found as a conic of revolution or second-order three-dimensional surface fitted to the observed magnetopause crossings [*Fairfield*, 1971; *Holzer and Slavin*, 1978; *Formisano et al.*, 1979; *Sibeck et al.*, 1991; *Roelof and Sibeck*, 1993]. Another frequent solution is the use of several different shapes simultaneously: *Kuznetsov and Suvorova* [1998] use two paraboloids that intersect at angle $\theta \approx 30^\circ$ (here, θ is an angle between X_{GSE} and the radius vector of the observed crossing); the *Petrinec and Russell* [1996] model (based on *Petrinec et al.* [1991] and *Petrinec and Russell* [1993]) employs two different functional forms for the dayside and nightside. *Shue et al.* [1997] introduced a new functional form characterized by two parameters, r_0 and α , representing the magnetopause standoff distance and the level of tail flaring. Depending on the amount of available data, the

shape parameters can be derived as functions of p_{sw} and for several subsets of data according to IMF B_z [Fairfield, 1971; Sibeck *et al.*, 1991] or can be bivariate functions of p_{sw} and IMF B_z [Roelof and Sibeck, 1993; Petrinec and Russell, 1996; Shue *et al.*, 1997, 1998].

[6] Another controlling factor of the magnetopause position is the orientation of the Earth's magnetic dipole axis, which is usually expressed as the dipole tilt angle λ in GSM coordinates [e.g., Spreiter and Briggs, 1962]. Spreiter and Briggs [1962] calculated magnetopause shapes in the meridian and equatorial planes in 5° increments of the dipole tilt angle. Even though they incorrectly assumed an elastic fluid interaction, the shape of the derived boundary was not significantly affected and the results clearly demonstrate varying cross section of the magnetosphere for different dipole tilt angles.

[7] Changes in the dipole orientation move the location of polar cusps [e.g., Wu, 1984; Tsyganenko, 1989] where the magnetopause is closer to the Earth due to lower magnetic field in these regions. The concept of a magnetic cusp dates back to MHD models in 1950s and 1960s [e.g., Berkowitz *et al.*, 1958; Grad and Hu, 1966]. Thus the presence of a magnetic cusp creates an indentation in the otherwise smooth dayside magnetopause which alters plasma flow around the magnetosphere. Petrinec and Russell [1995] indeed showed that the magnetopause shape is in fact dimpled on the dayside. The deepness of the indentation can reach $\sim 4 R_E$ and its location depends on the dipole tilt angle [Šafránková *et al.*, 2002]. Zhou and Russell [1997] used magnetopause crossings observed by Hawkeye to demonstrate that the cusp high-altitude location is controlled by the dipole tilt. Zhou *et al.* [1999] determined from Polar cusp observations that the cusp moves poleward to higher latitudes by roughly 1° for every 14° of tilt. Magion-4 cusp observations suggest an even more pronounced shift in latitude, approximately 1° for every 6.3° of tilt [Němeček *et al.*, 2000].

[8] Only a few magnetopause models have attempted to take into account the dipole tilt angle effects on the magnetopause shape. For example, Formisano [1979] attempted to make two-surface fits to magnetopause observations for $\lambda = 0^\circ$ and $\lambda = 20^\circ$, and Boardsen *et al.* [2000] developed an empirical model of the high-latitude magnetopause parameterized by p_{sw} , B_z , and λ . However, there is currently no global empirical magnetopause model which would adjust the boundary shape by the dipole tilt angle.

[9] The size and geometry of the magnetopause is a result of combined solar wind ram pressure, IMF orientation, and dipole tilt angle effects. The ram pressure effect scales the magnetopause size, while the IMF orientation and dipole tilt angle affect the geometry of the boundary. The tail magnetopause shape and position are also influenced by the IMF magnitude and solar wind plasma temperature because there the magnetic and thermal pressures are not negligible in the calculations of the pressure balance between lobes and solar wind plasma [e.g., Petrinec and Russell, 1996]. However, this is not a concern in our study, as we study bow shock cross section in the near-tail region where the bow shock shape is still primarily controlled by the dayside magnetopause [e.g., Spreiter *et al.*, 1966].

[10] Interaction of the supersonic solar wind with Earth's magnetosphere (magnetopause) creates fast mode magneto-sonic waves that travel back upstream, combine, and steepen to form the bow shock wave. The distance to the bow shock is then the sum of the magnetopause distance and the magnetosheath thickness. Thus it is reasonable to expect that the bow shock's shape and position depends on the same parameters as the obstacle. Indeed, theoretical calculations, numerical simulations, and observations confirm this expectation [e.g., Spreiter *et al.*, 1966; Fairfield, 1971; Formisano, 1979; Spreiter and Stahara, 1985; Farris *et al.*, 1991; Russell and Zhang, 1992; Farris and Russell, 1994; Cairns and Lyon, 1995; Cairns *et al.*, 1995]. It has been well established that the bow shock (and the magnetopause) scales with the solar wind ram pressure p_{sw} [Binsack and Vasyliunas, 1968; Formisano, 1979].

[11] The magnetosheath thickness, on the first order, is controlled by the upstream Mach numbers: sonic M_S , Alfvénic M_A , and magnetosonic M_{MS} . At low Mach numbers, the shock becomes weaker and the entire bow shock is found farther from Earth so that the deflection of the solar wind flow around the obstacle, the magnetopause, can still occur [e.g., Spreiter *et al.*, 1966; Farris and Russell, 1994]. The magnetosheath thickness increases at a higher rate for lower Mach numbers [Farris and Russell, 1994; Cairns and Grabbe, 1994; Fairfield *et al.*, 2001]. The bow shock should move to infinity as its amplitude asymptotically decreases as the upstream Mach number becomes 1. Nevertheless, a controversy still persist about how fast the bow shock standoff distance changes for low Mach numbers [Russell and Petrinec, 1996; Cairns and Grabbe, 1996; Petrinec and Russell, 1997; Dmitriev *et al.*, 2003]. Furthermore, numerical simulations by Spreiter and Rizzi [1974] found that the magnetosheath thickness actually decreases with decreasing Alfvénic Mach number M_A when $\theta_{Bv} = 0^\circ$ where θ_{Bv} is the angle between the IMF and solar wind velocity vectors. More recent two-dimensional (2-D) MHD simulations of the bow shock topology in field-aligned low- β flow around a perfectly conducting cylinder or sphere [De Sterck *et al.*, 1998; De Sterck and Poedts, 1999] showed that in the switch-on shock regime (roughly for $M_A < 2$ and $\beta < 0.7$) the nose of the shock becomes dimpled due to a complex multiple-shock front topology near the subsolar point. A cusp-like bow shock nose is also predicted by Kabin [2001]. The 3-D global ideal MHD simulations of Cairns and Lyon [1996] and Chapman *et al.* [2004], which model solar wind flow onto and around a hard, infinitely conducting boundary with location given by Farris *et al.* [1991], also found decreasing magnetosheath thickness at the subsolar point for very low values of M_A (less than ~ 2). On the basis of Interball-1 observations of the bow shock and the magnetopause, Merka *et al.* [2003b] reported an unusually thin magnetosheath, possibly the dimpled shock front, near the subsolar point for quasi-field-aligned solar wind flow. Furthermore, Slavin *et al.* [1996] found the radial distance of IMP 8 and WIND bow shock crossings only 80–85% of that predicted by models for $\theta_{Bv} < 20^\circ$.

[12] Theory and observations indicate that the bow shock asymptotically approaches the magnetosonic Mach cone [e.g., Landau and Lifshitz, 1959; Spreiter *et al.*, 1966; Slavin *et al.*, 1984]. This is the inclination angle that the

very distant shock makes with respect to the upstream velocity vector. It is interesting to note that the asymptotic Mach cone angle is not a constant value but varies with the IMF direction expressed by the IMF clock angle around the flow velocity vector [e.g., *Spreiter and Stahara*, 1985; *Verigin et al.*, 2003]. However, experimental studies have not found significant asymmetries for typical upstream conditions [*Slavin and Holzer*, 1981; *Slavin et al.*, 1984; *Bennett et al.*, 1997]. On the other hand, numerical simulations of *Chapman and Cairns* [2003] suggest substantial asymmetries of the bow shock's cross section due to various IMF orientations at low Alfvénic Mach numbers M_A with maximum asymmetry at $M_A = 1.9$.

[13] The shape of the bow shock depends on the obstacle's shape as demonstrated, for example, by the MHD bow shock simulations of *De Sterck and Poedts* [1999]. In case of terrestrial magnetopause, its dayside shape is well approximated by an ellipsoid, and therefore empirical bow shock models successfully describe the bow shock shape using second-order curves (conics) or surfaces [e.g., *Fairfield*, 1971; *Formisano*, 1979]. The requirement that the bow wave must asymptotically approach the Mach cone angle then leads to frequent use of the paraboloidal/hyperboloidal model geometry of the shock. Existing empirical bow shock models usually consider only the magnetopause standoff distance (for example, models discussed by *Merka et al.* [2003a]) instead of considering the shape of the obstacle. Even the few models that consider the obstacle's shape greatly simplify the shape of the magnetopause by taking into account only the nose curvature radius [*Farris and Russell*, 1994] and/or obstacle's bluntness [*Verigin et al.*, 2001].

[14] In summary, the bow shock position and shape are controlled by the obstacle size and shape, upstream Mach numbers, and IMF orientation. The obstacle (magnetopause) varies with the solar wind ram pressure p_{sw} , dipole tilt angle λ , and IMF magnitude and orientation. Out of all these parameters, the dipole tilt angle has not been considered for the parameterization of bow shock properties yet. We would like to emphasize that the present study is first, to our knowledge, to formally quantify the dipole tilt angle effect on bow shock cross section in the near tail.

[15] The present study employs a large database of IMP 8 bow shock crossings observed during 1973–2000 [*Merka et al.*, 2004]. The distribution of observed bow shock crossings is predominantly between 0 and $-20 R_E$ along the X_{GSE} axis and within $\pm 25 R_E$ in Z_{GSE} direction. Although this data distribution is not favorable for studying or modeling the entire bow shock shape, it is exceptionally well suited to study the bow shock's cross section(s) at the near magnetospheric tail. Section 2 describes the IMP 8 data set of bow shock crossings; section 3 explains the methodology employed to fit bow shock cross sections and to calculate error estimations. Distributions of the observed shock crossings with fitted elliptical bow shock cross sections for various solar wind or magnetospheric parameters are presented in section 4. The presented parameters are the dipole tilt angle λ , Alfvénic Mach number M_A , and the θ_{Bv} angle. Section 4 also compares the observations with results of 3-D global MHD magnetospheric/bow shocks simulations. The main part of the study, section 5, discusses the results in the context of previous work and their

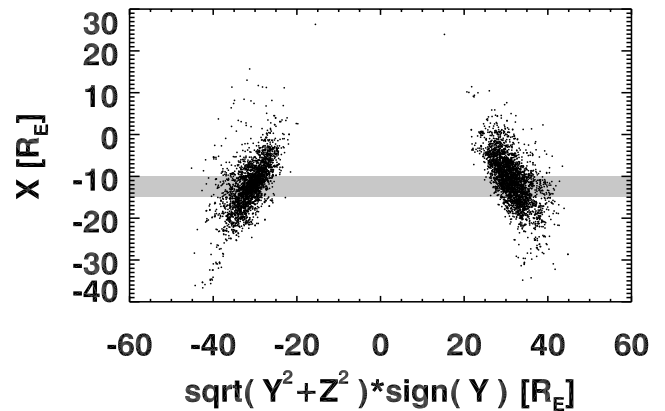


Figure 1. IMP 8 bow shock crossings observed during the years 1973–2000. The positions were normalized using equation (2) and are in Geocentric Plasma Ecliptic System (GPE) coordinates. The shaded area delimits positions $-15 R_E < X_{GPE} < -10 R_E$.

implications for future bow shock studies. Section 6 summarizes the results.

2. Data

[16] The present study employs the database of IMP 8 bow shock crossings created by *Merka et al.* [2004] that attempted to find all individual bow shock crossings observed by IMP 8 during the years 1973–2000. They classified the observed bow shocks by several criteria (for example, the data quality and/or availability) [*Merka et al.*, 2003a] and applied a uniform methodology to find all bow shock crossings. Out of the 11,455 records, 5870 unambiguous bow shock crossings, for which both upstream magnetic field and plasma measurements are available, form the foundation of the present study. These shock data are presented in Figure 1.

[17] *Merka et al.* [2004] reported a significant difference between plasma density measurements by the WIND and IMP 8 spacecraft and proposed to bring the IMP 8's measurement into agreement with the WIND's observations:

$$N_p^{\text{WIND}} = N_p^{\text{IMP8}} \cdot \left(\frac{1}{1.86 + 0.29 \cdot N_p^{\text{IMP8}}} + 0.73 \right), \quad (1)$$

where N_p^{IMP8} is plasma density measured by IMP 8 and N_p^{WIND} would be the plasma density as measured by WIND. In the present study, we adjust the IMP 8 observed plasma density to agree with WIND observations.

3. Calculation of the Bow Shock Cross Section

[18] Throughout the study, we employ several coordinate systems: GSE, GSM, GIPM, GPE, and GPM. The first two coordinate systems have been traditionally used in the solar wind and/or magnetospheric studies. However, the other three coordinate systems provide certain advantages for bow shock analysis. The solar wind flow changes directions, causing the magnetosphere and bow shock to be

blown in various directions, making comparisons of nonsimultaneous bow shock observations questionable. Therefore we rotate the GSE coordinate system so the solar wind impinging on the magnetosphere flows antiparallel to the X -axis while keeping the ecliptic north in the XZ plane. Note that this Geocentric Plasma Ecliptic System (GPE) also includes correction for the orbital motion of Earth. In solar wind/magnetospheric studies, aberrated GSE systems are often used causing some confusion about what exactly was aberrated. Thus we will use the acronym GPE to keep our definitions clear.

[19] Magnetospheric studies often employ the Geocentric Solar Magnetospheric System (GSM) that like the GSE system, has its X -axis pointing from Earth to Sun. The Y -axis is defined to be perpendicular to the Earth's magnetic dipole, so the X - Z plane contains the dipole axis. The orientation of the magnetic-dipole axis of Earth alters the otherwise cylindrical symmetry of the solar wind flow. Therefore we introduce the Geocentric Plasma Magnetospheric System (GPM) that like the GPE system, has its X -axis antiparallel to the impinging solar wind flow. The Y -axis is defined, like the GSM system, to be perpendicular to the Earth's magnetic dipole so that the XZ plane contains the dipole axis.

[20] The Geocentric Interplanetary Medium (GIPM) coordinates [Bieber and Stone, 1979] take into account variations due to different IMF orientations by rotating the coordinates so the IMF B_z component vanishes. Note that the solar wind flow is again antiparallel to the X -axis of the GIPM system in bow shock studies [e.g., Verigin *et al.*, 2003].

[21] The solar wind dynamic pressure scales the entire bow shock and the mechanism is reasonably well understood (see the introductory discussion in section 1). Therefore the observed positions r_o of the bow shock crossings were pressure-normalized according to the following equation [Formisano, 1979] in order to remove variations due to solar wind pressure variations before further analysis:

$$r_n = r_o \left(\frac{N_o v_o^2}{N_a v_a^2} \right)^{\frac{1}{5}}, \quad (2)$$

where N_o and v_o are the observed solar wind number density and bulk speed, respectively, with $N_a = 9.2 \text{ cm}^{-3}$, $v_a = 453 \text{ km/s}$ the average values for our list of bow shock crossings. Note that this normalization assumes that the dynamic pressure influences the size of the bow shock but not its shape. On the other hand, Petrinec and Russell [1996] showed that the solar wind thermal pressure p_t and IMF pressure p_m should be included in the pressure normalization resulting in non-self-similar scaling of the magnetopause. However, self-similar scaling defined by equation (2) is adequate for this study because shock shape at $X > -20 R_E$ is influenced predominantly by the dayside magnetopause, as can be seen, for example, from the Mach or characteristic lines in simulations of Spreiter *et al.* [1966].

[22] Upon removal of solar wind dynamic pressure effects, we sliced the data set into four subsets based on the bow shock crossing's position along the X -axis. Thus the value of

the X position can be in either of the following intervals: $(-20; -15)$, $(-15; -10)$, $(-10; -5)$, or $(-5; 0)R_E$. Overall, the best data coverage and the minimum orbital bias were found between -10 and $-15 R_E$ of X . Therefore we will present results based on this subset only. We note that the results from the other subsets are qualitatively the same but are less reliable or, in a few extremely bad cases, it is not possible to fit an ellipse to the particular subset at all due to lack of data to perform a statistically significant fit.

[23] In the next step, we independently selected the data based on various parameters (for example, extreme dipole tilt angles, low Mach numbers) as is discussed below. For each subset, best-fitting second-order curves, ellipses in particular, were derived according to the following procedure. A general equation of the second order curves (conics) is

$$F(y, z) = a_1 y^2 + 2a_2 yz + a_3 z^2 + 2a_4 y + 2a_5 z + a_6 = 0, \quad (3)$$

where (y, z) are the coordinates of a bow shock crossing and the free parameters $(a_1 \dots a_6)$ are determined by minimizing the root squared distance between the observed crossing and the conic. Thus the task is to minimize the merit function χ^2 defined by the relation

$$\chi^2 = \sum_{i=1}^n \left[\frac{F_i}{\sqrt{\nabla F_i}} \right]^2, \quad (4)$$

where n is the number of crossings at positions (y_i, z_i) . The Levenberg-Marquardt method [Marquardt, 1963] for nonlinear least squares fitting accomplishes this minimization. For more details about the implementation of the fitting method, the reader is referred to Appendix B of Peredo *et al.* [1993] and section 2 of Peredo *et al.* [1995].

[24] From the free parameters $(a_1 \dots a_6)$, we can derive the rotation of the ellipse by angle φ , the position of its center (y_0, z_0) , major semiaxis a , minor semiaxis b , and numerical eccentricity ϵ . The angle φ is defined

$$\tan(2\varphi) = \frac{2a_2}{a_1 - a_3}, \quad (5)$$

the center's position (y_0, z_0) can be found by solving the equations

$$a_1 y_0 + a_2 z_0 = -a_4, \quad (6)$$

$$a_2 y_0 + a_3 z_0 = -a_5. \quad (7)$$

The major and minor semiaxes, a and b , respectively, can be found from comparing the normal form of an ellipse to its central representation. Numerical eccentricity ϵ is given by the formula $b^2 = a^2(1 - \epsilon^2)$.

[25] The standard errors of the fitted parameters were estimated by the bootstrap method proposed by Efron [1979]. The bootstrap method is a general methodology for nonparametrically estimating the statistical errors and the implementation is quite straightforward [see Kawano and Higuchi, 1995]. The number of bootstrap trials M , an

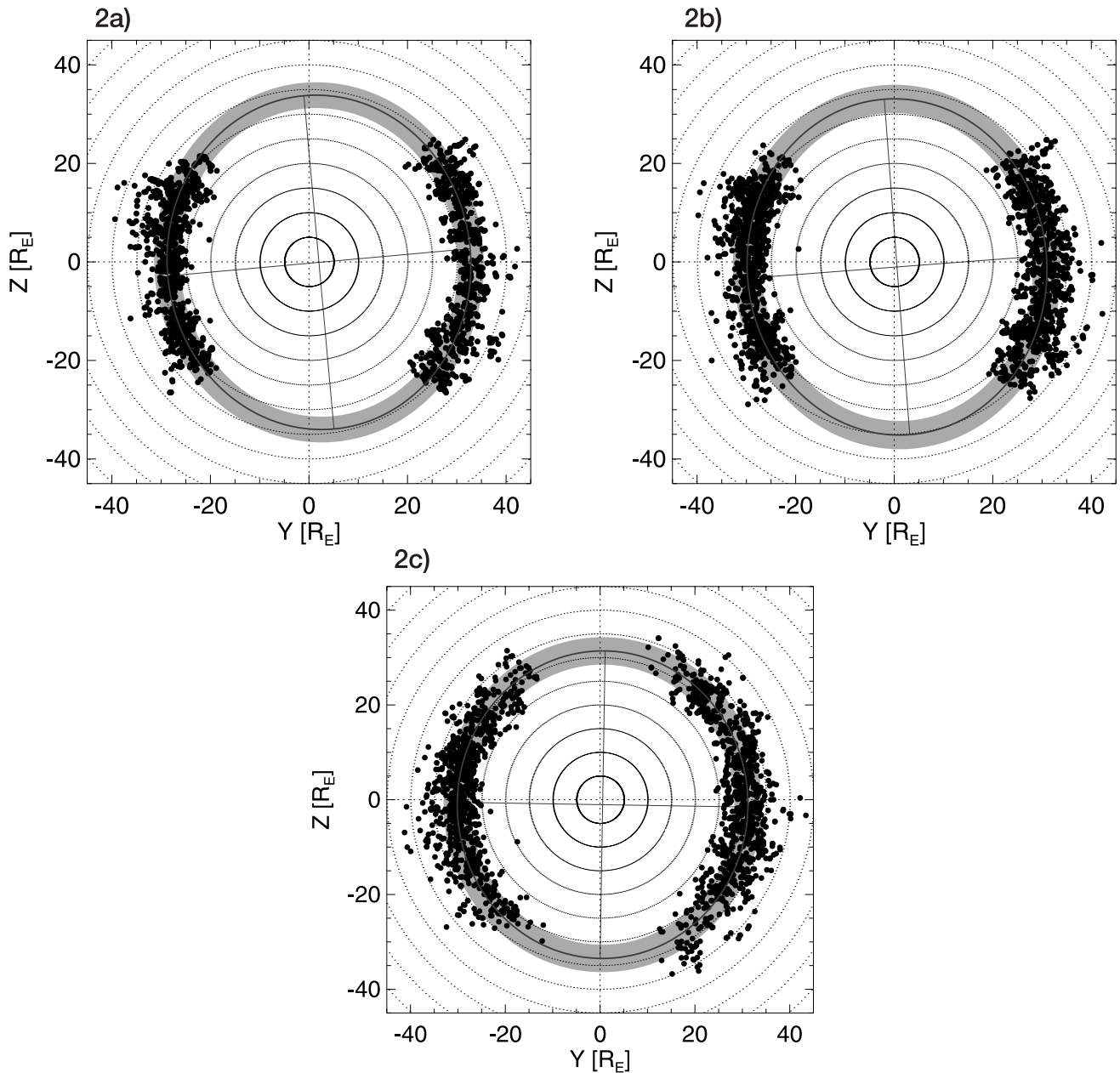


Figure 2. The best-fit ellipse (the gray curve and the shaded area) to the bow shock crossings (the dots) observed at $X \in (-15; -10) R_E$ in (a) Geocentric Solar Ecliptic System (GSE), (b) GPE, and (c) Geocentric Plasma Magnetospheric System (GPM) coordinates.

ad hoc parameter, usually does not exceed 2000 [Kawano and Higuchi, 1995, and references therein]. However, in this study we set $M = 10^4$ in order to obtain very reliable results.

4. Bow Shock's Cross Section

[26] The best fits of an ellipse to the bow shock crossings in GSE, GPE, and GPM coordinates are displayed in Figure 2. The gray band delimits an area from $r - \sigma$ to $r + \sigma$, where r is radial distance from the origin to the ellipse (the heavy dark gray curve) and σ is the

standard error of the data distribution around the ellipse. Here σ is given as

$$\sigma = \sqrt{\frac{\sum_{i=1}^n (r_i^{\text{BS}}(\phi_i) - r_i(\phi_i))^2}{n-1}}, \quad (8)$$

where $r_i(\phi_i)$ and $r_i^{\text{BS}}(\phi_i)$ are radial distances to the ellipse and the i th bow shock crossing, respectively, for the polar angle ϕ_i . The standard error σ serves as a convenient estimator of the data point spread around the fitted curve. In Figure 2 the ellipse's semimajor and semiminor axes are

Table 1. Parameters $a_1 \dots a_6$ for Best Fitting Elliptical Bow Shock Cross Sections for Various Conditions

	a_1	a_2	a_3	a_4	a_5	a_6
GSE	1.028 ± 0.005	0.016 ± 0.005	0.849 ± 0.024	-2.083 ± 0.062	0.039 ± 0.144	-973.3 ± 3.7
GPE	1.036 ± 0.006	0.016 ± 0.006	0.823 ± 0.030	-0.571 ± 0.066	0.832 ± 0.161	-957.6 ± 3.9
GPM	1.021 ± 0.005	-0.002 ± 0.006	0.911 ± 0.016	-0.540 ± 0.069	0.954 ± 0.138	-958.3 ± 3.9
GPM, $\lambda < -15^\circ$	1.003 ± 0.010	-0.019 ± 0.010	0.943 ± 0.030	-0.497 ± 0.125	2.745 ± 0.255	-987.0 ± 7.4
GPM, $-10^\circ < \lambda < 10^\circ$	1.042 ± 0.007	0.014 ± 0.009	0.838 ± 0.024	-0.444 ± 0.112	0.875 ± 0.214	-936.5 ± 6.2
GPM, $\lambda > 15^\circ$	0.997 ± 0.012	0.030 ± 0.015	1.000 ± 0.047	-0.662 ± 0.175	-0.938 ± 0.365	-967.1 ± 9.3
GPM, $5 < M_A < 8$	1.002 ± 0.010	0.011 ± 0.012	0.978 ± 0.028	-1.109 ± 0.149	1.584 ± 0.270	-991.2 ± 8.4
GPM, $M_A > 10$	1.024 ± 0.006	-0.003 ± 0.008	0.885 ± 0.025	-0.271 ± 0.087	0.329 ± 0.198	-928.4 ± 4.9
GPM, $M_A < 7, M_s < 7$	1.039 ± 0.023	-0.025 ± 0.024	0.904 ± 0.054	-1.404 ± 0.345	2.239 ± 0.532	-1058.8 ± 19.1
GPM, $M_A > 7, M_s > 7$	1.026 ± 0.005	-0.011 ± 0.007	0.890 ± 0.020	-0.383 ± 0.080	0.650 ± 0.166	-946.6 ± 4.4
GPM, $\theta_{Bv} < 20^\circ$	1.027 ± 0.011	-0.013 ± 0.018	0.883 ± 0.054	0.093 ± 0.166	0.355 ± 0.393	-854.7 ± 9.0
GPM, $\theta_{Bv} > 45^\circ$	1.020 ± 0.006	0.000 ± 0.008	0.913 ± 0.021	-0.658 ± 0.090	1.132 ± 0.188	-996.7 ± 5.1
GIPM, $5 < M_A < 8$	1.007 ± 0.012	0.023 ± 0.013	0.990 ± 0.016	-0.443 ± 0.187	-0.229 ± 0.210	-984.7 ± 8.8
GIPM, $M_A > 10$	1.019 ± 0.008	0.009 ± 0.007	0.980 ± 0.008	0.186 ± 0.121	0.029 ± 0.109	-928.8 ± 4.9

also displayed for easy recognition of its eccentricity and orientation. The fitted parameters ($a_1 \dots a_6$) together with their estimated errors based on the bootstrap method are presented in Table 1. The other derived parameters of the best-fit ellipses (φ , y_0 , z_0 , a , b , ε , and σ) can be found in Table 2 along with the number of data points for all investigated subsets.

[27] Note the lack of data coverage in arcs subtending nearly 90° in the north-south directions in the GSE and GPE coordinates. The data coverage is significantly better in GPM coordinates where the lack of coverage is reduced to arcs subtending only 45° in the north-south directions. Therefore the semimajor axis a calculated in the GPM coordinates is closer to the real distance to the bow shock along the Z axis than values obtained in GSE and GPE coordinates in spite of the highly reliable fits in all cases (Tables 1 and 2). The ellipse's center is more displaced in the GSE coordinates due to the orbital and solar wind flow aberrations.

[28] The GPM coordinate system is the most suitable system to study dipole tilt angle effects. Therefore Figure 3 displays changes of the bow shock's cross section at $X \in (-15; -10) R_E$ in the GPM coordinates for different values of the dipole tilt angle: (Figure 3a) $\lambda < -15^\circ$, (Figure 3b) $-10^\circ < \lambda < 10^\circ$, and (Figure 3c) $\lambda > 15^\circ$. Note that the cross section moves up and down along the Z -axis when the dipole tilt changes. In Figure 3 we can see that the shock cross section moves southward (northward) for large negative (positive) tilt angles λ (see also Table 2). The observed

difference between the extreme north and south positions is about $3.8 R_E$ at $X \in (-15; -10) R_E$ (the shift of the ellipse's center).

[29] For comparison, we present results obtained from global 3-D MHD magnetospheric simulations (the BATSRUS model) run at the Community Coordinated Modeling Center (CCMC, available at <http://ccmc.gsfc.nasa.gov>) in Figure 4. Figure 4 shows the total current J calculated by the MHD model. The display of the current J clearly presents the bow shock (outer oval) and the magnetopause boundaries ($\nabla \times \mathbf{B}$). We note that the variances in the current intensity and the width of the current layer are due to different densities of the simulation grid. The simulations were performed for solar wind plasma density $N = 9.2 \text{ cm}^{-3}$, upstream bulk velocity $\mathbf{v} = (-453, 0, 0) \text{ km/s}$, proton temperature $T = 2.321 \cdot 10^5 \text{ K}$, and IMF $\mathbf{B} = (0, 0, 5) \text{ nT}$ in GSM coordinates. The choice of solar wind flow along the X axis means that in this particular case, the GSM coordinate system is identical to GPM. Note that the selected plasma density N and bulk velocity \mathbf{v} correspond to the average conditions in the IMP 8 data set. The northward IMF orientation was chosen in order to avoid possible complications in the numerical treatment of magnetic reconnection on the dayside magnetopause for southward IMF. Comparison of Figures 3 and 4 shows the same response of the bow shock to different dipole tilts with even the magnitude of the shift $\sim 4 R_E$ in close agreement.

[30] We have also selected bow shock crossings based on the upstream sonic M_s and Alfvénic M_A Mach numbers and

Table 2. Parameters φ , y_0 , z_0 , a , b , ε , and σ for Best-Fitting Elliptical Bow Shock Cross Sections for Various Conditions; N is the Number of Data

	φ , deg	y_0, R_E	z_0, R_E	a, R_E	b, R_E	ε	σ, R_E	N
GSE	5.2 ± 1.9	2.0 ± 0.1	-0.1 ± 0.2	34.0 ± 0.5	30.8 ± 0.1	0.421 ± 0.032	2.6	1861
GPE	4.3 ± 1.7	0.6 ± 0.1	-1.0 ± 0.2	34.2 ± 0.6	30.4 ± 0.1	0.455 ± 0.036	2.9	2041
GPM	-0.9 ± 3.3	0.5 ± 0.1	-1.0 ± 0.2	32.4 ± 0.3	30.7 ± 0.1	0.328 ± 0.030	2.9	2041
GPM, $\lambda < -15^\circ$	-16.0 ± 14.3	0.4 ± 0.1	-2.9 ± 0.3	32.6 ± 0.5	31.4 ± 0.2	0.265 ± 0.054	2.6	542
GPM, $-10^\circ < \lambda < 10^\circ$	4.0 ± 2.7	0.4 ± 0.1	-1.1 ± 0.3	33.5 ± 0.5	30.0 ± 0.1	0.444 ± 0.032	2.8	708
GPM, $\lambda > 15^\circ$	46.2 ± 25.6	0.6 ± 0.2	0.9 ± 0.4	31.6 ± 0.5	30.7 ± 0.4	0.243 ± 0.058	3.0	329
GPM, $5 < M_A < 8$	20.7 ± 33.7	1.1 ± 0.2	-1.6 ± 0.3	32.0 ± 0.4	31.5 ± 0.2	0.179 ± 0.060	3.2	613
GPM, $M_A > 10$	-1.2 ± 3.8	0.3 ± 0.1	-0.4 ± 0.2	32.4 ± 0.5	30.1 ± 0.1	0.368 ± 0.039	2.4	834
GPM, $M_A < 7, M_s < 7$	-10.1 ± 15.9	1.3 ± 0.3	-2.4 ± 0.6	34.4 ± 1.0	32.0 ± 0.4	0.372 ± 0.083	3.5	131
GPM, $M_A > 7, M_s > 7$	-4.4 ± 3.3	0.4 ± 0.1	-0.7 ± 0.2	32.6 ± 0.4	30.4 ± 0.1	0.366 ± 0.032	2.6	1214
GPM, $\theta_{Bv} < 20^\circ$	-5.0 ± 11.4	-0.1 ± 0.2	-0.4 ± 0.4	31.1 ± 0.9	28.8 ± 0.2	0.378 ± 0.068	2.0	177
GPM, $\theta_{Bv} > 45^\circ$	0.2 ± 4.5	0.6 ± 0.1	-1.2 ± 0.2	33.1 ± 0.4	31.3 ± 0.1	0.324 ± 0.038	2.9	1266
GIPM, $5 < M_A < 8$	34.3 ± 20.1	0.4 ± 0.2	0.2 ± 0.2	31.8 ± 0.2	31.0 ± 0.2	0.218 ± 0.048	3.5	613
GIPM, $M_A > 10$	11.9 ± 11.8	-0.2 ± 0.1	-0.0 ± 0.1	30.8 ± 0.1	30.2 ± 0.1	0.204 ± 0.036	2.4	834

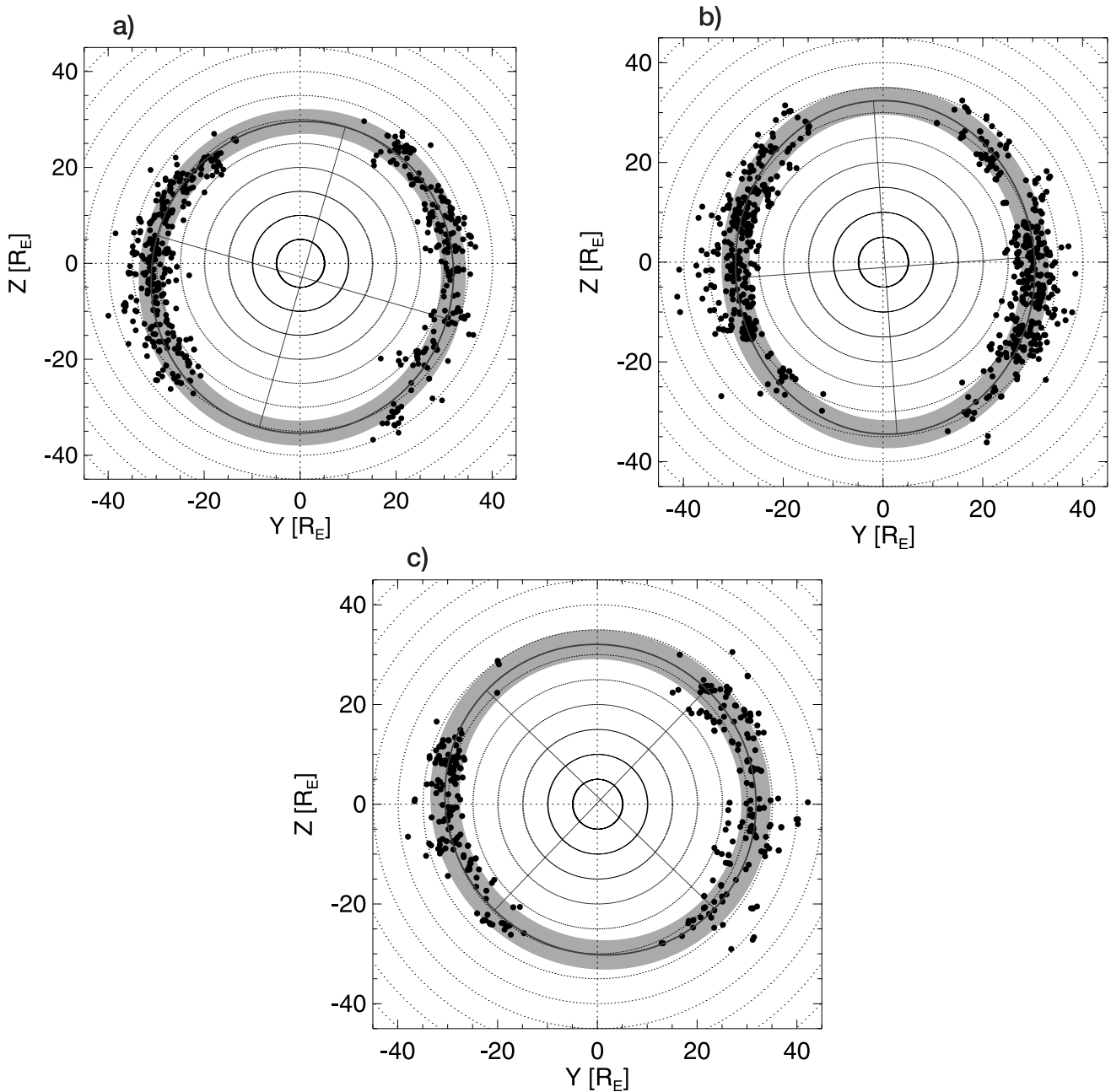


Figure 3. Bow shock's cross section at $X \in (-15; -10) R_E$ in the GPM coordinates for various dipole tilt angles λ : (a) $\lambda < -15^\circ$, (b) $-10^\circ < \lambda < 10^\circ$, and (c) $\lambda > 15^\circ$. Note the up and down movement of the cross section.

studied their distributions in GPM and GIPM coordinates. The bow shock standoff distance greatly increases for low Mach numbers which, together with the orbital trajectory of IMP 8, limits the number of low-Mach-number bow shock crossings in our data set, especially in the region of X from -10 to $-15 R_E$. Therefore we can only compare bow shock crossings observed for midrange Mach numbers (5–8) with cases of high Mach numbers (greater than 10) (Figure 5 and Tables 1 and 2). Tables 1 and 2 also present parameters of the best fits in both GPM and GIPM coordinates for selections based on the values of the upstream Mach numbers: $5 < M_A < 8$; $M_A > 10$; $M_A < 7$ and $M_s < 7$;

$M_A > 7$ and $M_s > 7$. The comparison of Figures 5a and 5b, and also the values presented in Table 2, shows that the bow shock's cross section is smaller for higher values of upstream Mach numbers and that the scatter of points around the best fit is significantly reduced (by $\approx 1 R_E$). Furthermore, except for the θ_{Bv} effect described in the following paragraph, we did not find any conclusive IMF dependence in Figure 5, which should be easy to discover in the GIPM coordinates, where the IMF is pointing only in the $+Y$ direction [Bieber and Stone, 1979].

[31] Figure 6 compares bow shock's cross sections for IMF quasi-aligned with or quasi-perpendicular to the solar

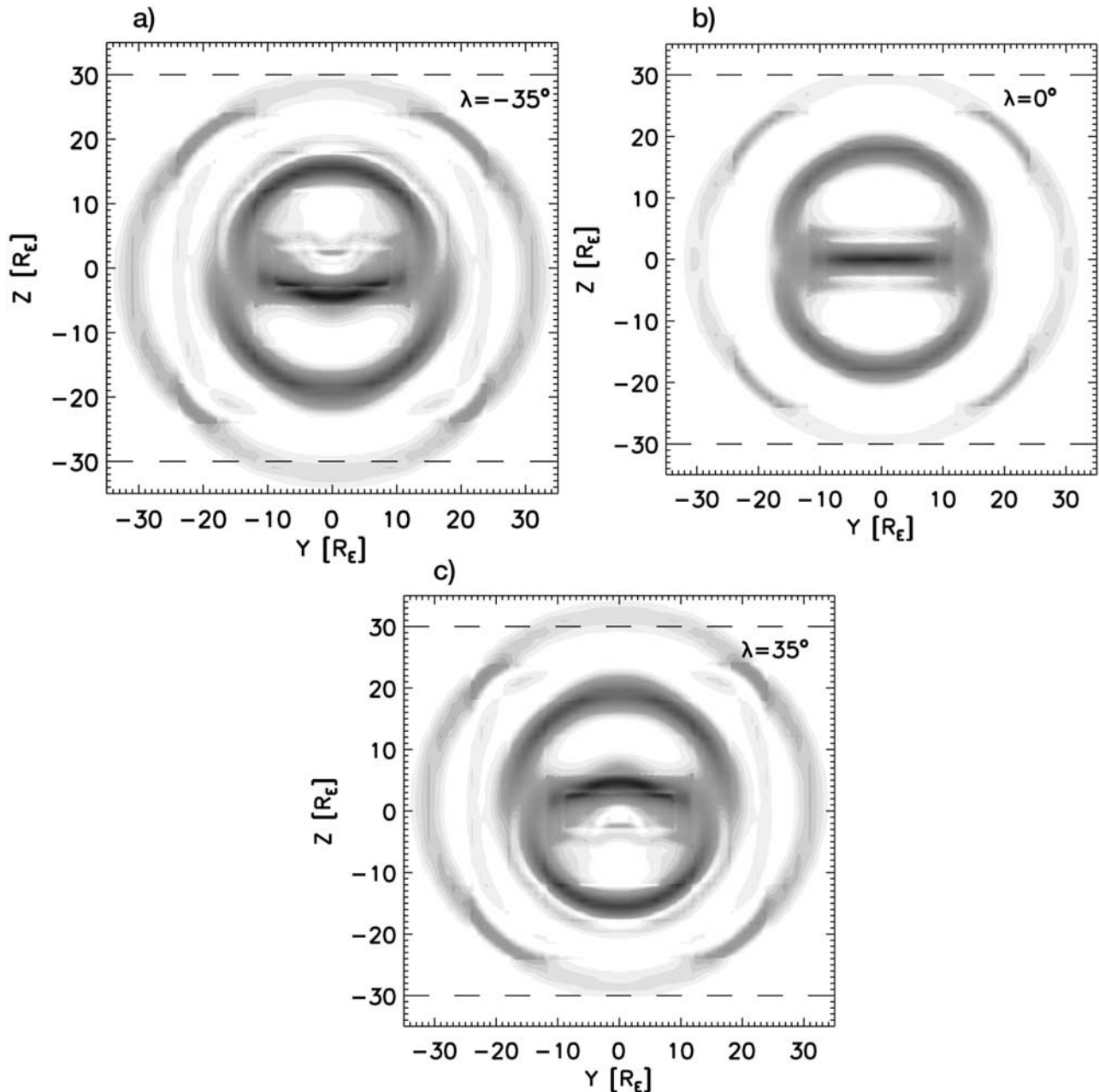


Figure 4. Bow shock's cross section, represented by the outer current layer displayed, in GSM/GPM coordinates at $X_{\text{GSM}} = -10 R_E$ as predicted by global three-dimensional (3-D) MHD simulations for three different dipole tilt angles λ : (a) $\lambda = -35^\circ$, (b) $\lambda = 0^\circ$, and (c) $\lambda = 35^\circ$. The intensity of the total current J is depicted by the shading. The inner oval represents the magnetopause and the horizontal feature is the cross-tail current. Note the up and down movement of the cross section.

wind flow: $\theta_{\text{BV}} < 20^\circ$ or $\theta_{\text{BV}} > 45^\circ$. The bow shock appears to be closer to the X -axis and the data scatter is lower when the IMF is aligned with the upstream flow (see Figure 6 and Table 2).

5. Discussion

[32] We have attempted to describe the bow shock's cross section in several coordinate systems because some of them have been traditionally used (GSE, GSM) and some are more natural for the description of the bow shock/magnetosphere

due to the underlying physics and symmetries (GIPM, GPE, GPM). In particular, the GIPM, GPE and GPM systems rotate the coordinates so that the solar wind bulk velocity is antiparallel to the X -axis. This is natural and physically reasonable because the blowing solar wind shapes and orients the magnetosphere. The GIPM or GPM coordinate frames attempt to accentuate the IMF orientation or the dipole tilt angle effects on the magnetosphere/bow shock system. Even though the GSM coordinates are commonly employed in space physics, we argue, based on the results discussed in detail below, that the GPM coordinate system

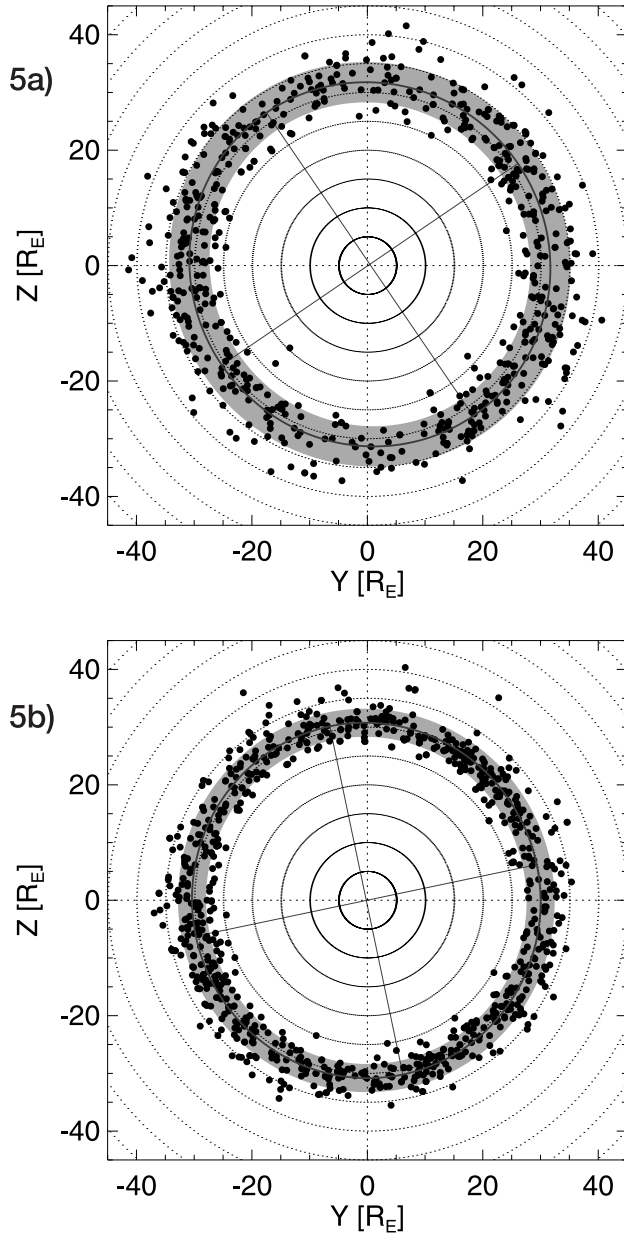


Figure 5. Bow shock's cross section at $X \in (-15; -10) R_E$ in the GPM coordinates for selected values of the upstream Alfvénic Mach number M_A : (a) $5 < M_A < 8$ and (b) $M_A > 10$.

should be used for magnetopause and bow shock studies. In our particular case, the GPM coordinates also provide the added benefit of improving the data coverage around the bow shock's cross section (Figure 2).

[33] Magnetospheric studies usually take into account the orientation of the Earth's dipole. However, frequently used global magnetopause or bow shock models [e.g., Merka *et al.*, 2003a; Šafránková *et al.*, 2002, and references therein] ignore this effect even though it is well known that changes in the obstacle's (magnetopause) shape will result in different bow shock shapes/positions [e.g., Farris and Russell, 1994; De Sterck and Poedts, 1999]. Indeed, the IMP 8 observations confirm this intuitive conclusion, as demonstrated in Figure 3 and Table 2. The shock's cross section, its center in particular, moves by $3.8 R_E$ at $X = -10$

to $-15 R_E$ between extremely positive and negative dipole tilt angles λ (see the parameter z_0 in Table 2). Also the area of the shock's cross section is larger (the semimajor axes are larger) for negative than for positive tilts. However, this appears to be due to the data coverage, as for the subsets with extremely positive or negative tilts a mirror symmetry around the XY plane is expected on the first order. Note that other effects, as for example the IMF orientation effects on both the bow shock and the magnetopause, will cause slight deviations from the mirror symmetry. The north-south diameter of the cross section for $-10^\circ < \lambda < 10^\circ$ is larger than for the other two cases. In fact, the southernmost (northernmost) locations for $-10^\circ < \lambda < 10^\circ$ and $\lambda < -15^\circ$ ($\lambda > 15^\circ$) are practically identical (see Figure 3). This effect is most likely caused by the

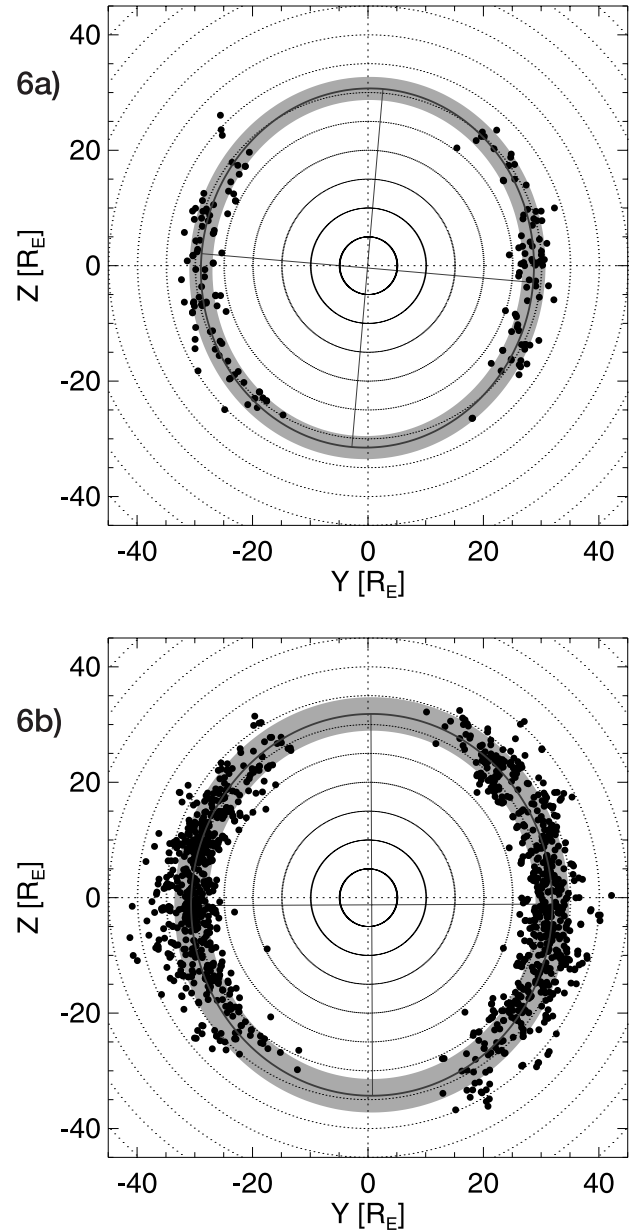


Figure 6. Bow shock's cross section at $X \in (-15; -10) R_E$ in the GPM coordinates for different values of the θ_{BV} angle: (a) $\theta_{BV} < 20^\circ$ and (b) $\theta_{BV} > 45^\circ$.

presence of both, although small, positive and negative tilts in the subset $-10^\circ < \lambda < 10^\circ$. Indeed, the north-south size of the cross section decreased by $\approx 1 R_E$ when we selected points with $-5^\circ < \lambda < 5^\circ$ instead of $-10^\circ < \lambda < 10^\circ$ but with poorer statistics.

[34] In spite of small errors in the best fits (Tables 1 and 2), the gaps in data coverage in the north/south directions might cast some doubts on the validity of the presented results. Therefore we have requested simulation runs of the global 3-D MHD magnetospheric model BATSURUS at the CCMC for three different orientations of the Earth's dipole axis: Figure 4 displays cuts through the simulation domain at $X_{GSM} = -10 R_E$ and the displayed parameter is the total current J which easily reveals the bow shock and magnetopause boundaries. Comparison of Figures 3 and 4 reveals a striking similarity in the bow shock's response to the extremely positive or negative tilt angles λ . Note that for $\lambda = 0^\circ$ the bow shock's cross section is slightly smaller.

[35] As we have already mentioned above, the observed changes in the bow shock's cross section are caused by changes in the magnetopause shape. When the dipole angle increases, the magnetospheric cross section (in the YZ plane) increases and its center in the tail moves below (above) the X -line for negative (positive) tilt angles λ [see Spreiter and Briggs, 1962]. In Figure 7 the global 3-D MHD simulations provide more information about how the shock's shape is affected by the dipole tilt. In order to aid the eye, a heavy black bar is plotted at $X = -10 R_E$ and from $Z = -30$ to $30 R_E$. This bar would represent the diameter of a hypothetical, axially symmetric bow shock that does not change with λ . Note that the bar also represents the XZ cut through the YZ cross sections presented in this study. The two outer current layers in Figure 7 represent the bow shock and the magnetopause and we can also easily recognize the magnetospheric cusps. Note the north (south) displacement of both the bow shock and magnetopause for large positive (negative) tilt angles λ on the nightside. However, significant changes in shape/position of at least $1 R_E$ are not only limited to the region downstream from the cusps but can be also seen at the dayside magnetopause and bow shock. Therefore the dependence on the dipole tilt should be included in both bow shock and magnetopause models. A bow shock model without explicit dependencies on dipole tilt angle can be still valid, as long as it has a dependency upon a magnetopause model which in turn is dependent upon the dipole tilt angle. We would like to note that theoretical calculations generally take λ into account [e.g., Spreiter and Briggs, 1962] but the authors are not aware of any global empirical bow shock or magnetopause model accounting for the λ dependence except the unfinished magnetosphere/magnetopause model by Tsyganenko [2002a, 2002b] and attempts by Formisano *et al.* [1979] to make two-surface fits to magnetopause observations for $\lambda = 0^\circ$ and $\lambda = 20^\circ$.

[36] The Mach number dependences have also been investigated in spite of the shortage of low-Mach-number bow shock crossings in the IMP 8 database. Figure 5 compares, in GIPM coordinates, bow shock crossings observed for $5 < M_A < 8$ to crossings with $M_A > 10$ where M_A is the Alfvénic Mach number. The bow shock cross section is slightly larger for lower Alfvénic Mach numbers: Both semimajor and semiminor axes are greater by $\approx 1 R_E$.

The larger bow shock distance for lower Mach numbers is a well-known behavior even though some controversies still exist [Spreiter *et al.*, 1966; Farris and Russell, 1994; Cairns and Grabbe, 1994; Russell and Petrinec, 1996; Cairns and Grabbe, 1996; Petrinec and Russell, 1997; Fairfield *et al.*, 2001]. We have investigated the bow shock shape in response to changing sonic and Alfvénic Mach numbers M_s , M_A and found the shock cross section larger for lower Mach numbers in each case (Figure 5 and Table 2). We also note the substantially higher scatter σ of the data points for lower Mach numbers, the differences in scatter are approximately $1 R_E$ between the lower and higher Mach number cases (Table 2). We explain this difference by the higher sensitivity of the bow shock's position to the same degree of change in the Mach number when the upstream Mach number is low [Farris and Russell, 1994; Cairns and Lyon, 1995; Fairfield *et al.*, 2001].

[37] Note the nearly circular cross section of the bow shock in Figure 5. In the GIPM coordinates, we might expect to see the IMF effects on the bow shock's shape as the bow wave approaches the Mach cone in infinity [Michel, 1965]. The Mach cone angle is not axially symmetric and depends on the IMF orientation [Verigin *et al.*, 2003]. However, at $X = -10 R_E$, it appears that the bow shock's shape and position are determined primarily by the obstacle's shape in agreement with Slavin and Holzer [1981], though the data points are scattered, thus possibly masking small asymmetry effects. In particular, the asymptotic bow shock's cross section should be elongated along the Z axis of the GIPM coordinates and/or the shock should extend farther in the $+Y$ than in the $-Y$ directions [see Verigin *et al.*, 2003]. We, however, believe that the observed scatter is primarily due to the bow shock crossings observed when the magnetosphere-bow-shock system was not in its equilibrium state. With a large enough sample set, as we believe the IMP 8 shock data set is, we expect just as many outbound shock crossings as inbound crossings, so the time lag effects of the shock moving to its equilibrium state, which ultimately translate as spatial coordinate effects, will cancel out. Recent MHD simulations of Chapman and Cairns [2003] and Chapman *et al.* [2004] have shown that significant asymmetries in bow shock cross section develop when $M_A < 3$. However, the IMP 8 database does not contain enough data points in this range of M_A to allow an investigation of those asymmetries.

[38] The present study confirms the smaller size of the bow shock cross section when $\theta_{Bv} < 20^\circ$ (Figure 6 and Table 2): The semiminor axis b (roughly the flank standoff distance) is shorter by 8% and the semimajor axis a is shorter by 6%. Note the higher uncertainty of the a values because of the data gap in the north/south directions (Figure 6). Owing to the similarity between the θ_{Bv} and M_A results, we checked the subset $\theta_{Bv} < 20^\circ$ for the values of M_A and found that 19% of points were observed for $M_A < 8$ or 53% for $M_A < 10$ (out of 177 data points). This leads us to the conclusion that the observed θ_{Bv} effect is real and independent of the M_A effect. The θ_{Bv} effect has been indeed reported by two studies: Slavin *et al.* [1996] suggested that magnetosheath thickness may decrease by $\sim 10\%$ as the IMF becomes increasingly flow-aligned, and Merka *et al.* [2003b] reported an unusually thin magnetosheath during a prolonged period of $\theta_{Bv} < 15^\circ$ at the

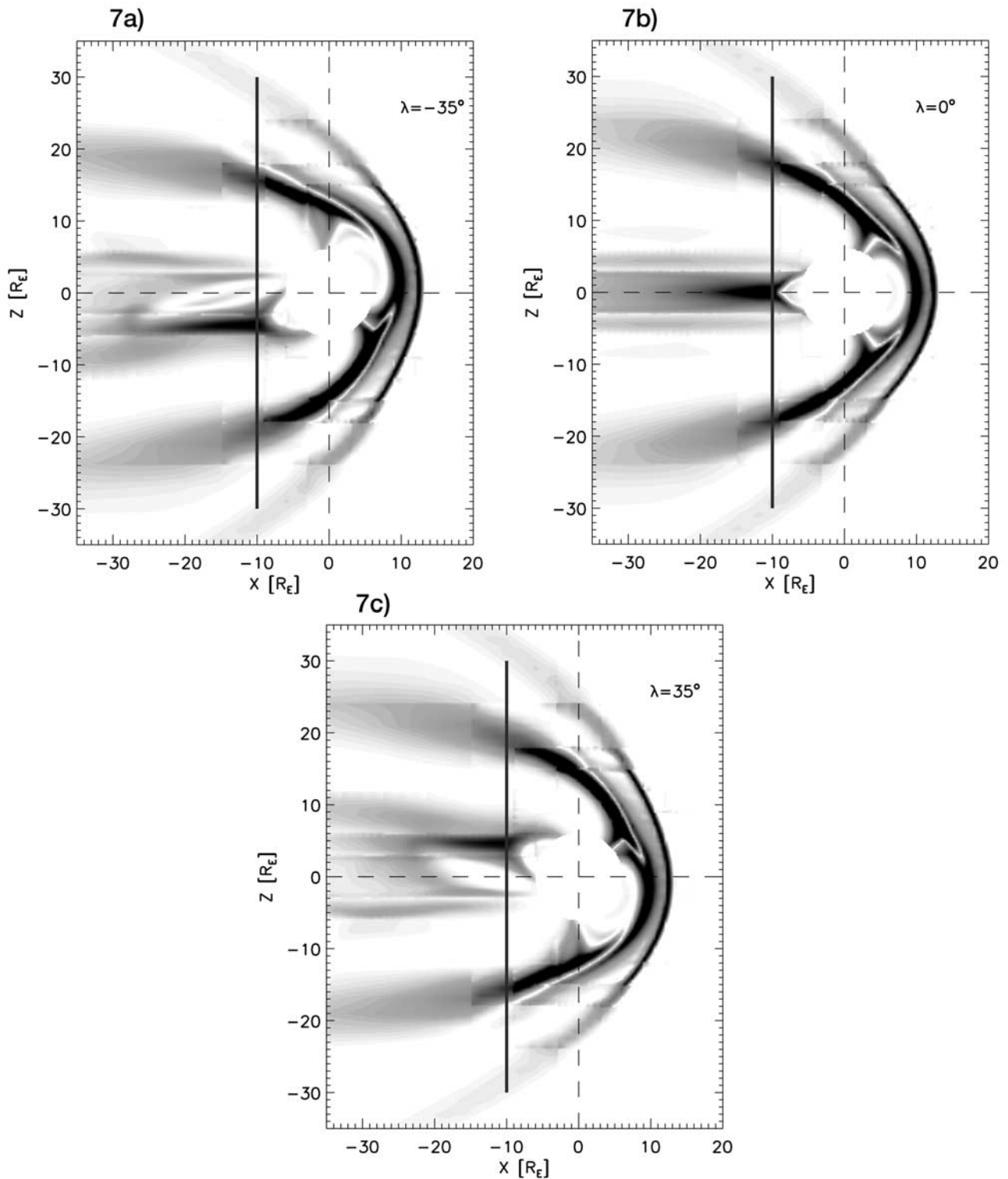


Figure 7. Total current predicted by global 3-D MHD simulations in GSM/GPM coordinates for three different dipole tilt angles λ : (a) $\lambda = -35^\circ$, (b) $\lambda = 0^\circ$, and (c) $\lambda = 35^\circ$. The outer current layer corresponds to the bow shock, the inner layer is the magnetopause, and along the X axis are the tail currents. The heavy black bar depicts a $60 R_E$ diameter of a hypothetical bow shock's cross section with axial symmetry at $X_{GSM} = -10 R_E$.

subsolar point. We assume that this effect is caused by a change in the obstacles shape/size and/or by thinning magnetosheath as demonstrated for extremely low-Mach-number conditions in numerical MHD simulations [De

Sterck *et al.*, 1998; De Sterck and Poedts, 1999; Chapman *et al.*, 2004]. However, note that the MHD simulations found thinner magnetosheath only at certain locations, namely the dimpled bow shock at the subsolar point, and

only for extremely low upstream Alfvénic Mach number values [De Sterck *et al.*, 1998; De Sterck and Poedts, 1999; Chapman *et al.*, 2004]. Thus the MHD simulations do not fully explain the observed θ_{Bv} effect at the magnetospheric flanks that we have clearly demonstrated even for significantly larger Mach numbers (Figure 6). The magnetopause shape changes may be caused by the magnetic pressure increase at the magnetospheric flanks when $\theta_{Bv} \rightarrow 0^\circ$ or by the magnetic field pile-up, producing increased pressure at the subsolar region and making the obstacle blunter for $\theta_{Bv} > 20^\circ$ [Petrinec and Russell, 1996, 1997]. On a final note, the almost 1 R_E difference in the scatter for the two θ_{Bv} subsets suggests higher variability of the bow shock's position for $\theta_{Bv} > 45^\circ$.

[39] The observed scatter σ around the best-fit ellipses (Table 2) can be attributed to several contributing factors: (1) the bow shock crossings are not, in general, observed when the shock wave is in equilibrium position; (2) we hold only a few parameters fixed at a time and thus other parameters probably contribute to the scatter; (3) the distance of the shock from the X -axis increases by approximately 2.5 R_E in the interval of $X \in (-15; -10) R_E$ (see Figure 1) which alone contributes up to 1.25 R_E to σ , depending on the data distribution within the interval.

6. Summary

[40] In the study, we have employed a list of 5870 bow shock crossings observed by the IMP 8 spacecraft during the years 1973–2000 and we have studied the response of the bow shock's cross section at $-15 R_E < X < -10 R_E$ to selected magnetospheric (dipole tilt angle λ) and upstream parameters (IMF, upstream Mach numbers, θ_{Bv}). Note that the solar wind dynamic pressure dependence and variations in the solar wind flow directions were removed prior to the analysis by pressure scaling (equation (2)) the positions and by the choice of the coordinate system(s) in which the upstream flow is antiparallel to the X -axis.

[41] The present results demonstrate that the Earth's dipole tilt angle λ is an important parameter for bow shock models. We have shown that the shock's cross section moves by 3.8 R_E in the north-south direction when the dipole tilts toward and away from the Sun. Although the importance of the λ parameter is appreciated in magnetospheric studies and in theoretical descriptions of the magnetopause, it is not used in current magnetopause or bow shock models. A quick review of global 3-D MHD simulations has confirmed the IMP 8 observations and, furthermore, it suggests the importance of the dipole tilt angle even for the dayside bow shock.

[42] We have found, in agreement with previous theoretical and experimental studies, the bow shock's cross section to shrink for higher upstream Mach numbers. A lower scatter of the bow shock crossings has been observed for higher Mach numbers in agreement with the theories suggesting greater sensitivity (or greater movement) of the shock wave in cases of lower Mach numbers. Except for the θ_{Bv} effect, we have not found any significant IMF orientation effects on the bow shock.

[43] A few studies [Slavin *et al.*, 1996; Merka *et al.*, 2003b] reported the bow shock wave closer to Earth than expected when the IMF was nearly aligned with the solar

wind flow ($\theta_{Bv} < 20^\circ$). Therefore this effect has been investigated and confirmed: The major and minor semiaxes are shorter by 6% and 8%, respectively, for $\theta_{Bv} < 20^\circ$ in comparison with $\theta_{Bv} > 45^\circ$. The reason is yet unclear but some theoretical considerations suggest changes in the total pressure around the magnetopause depending on the IMF orientation [Petrinec and Russell, 1996, 1997].

[44] Although more research is still needed, and especially high-latitude bow shock observations would be very beneficial, this study provides an experimental confirmation that both the dipole tilt angle λ and the IMF orientation with respect to the solar wind flow θ_{Bv} should be considered in future bow shock (and possibly magnetopause) models.

[45] **Acknowledgments.** This work was performed while the author J. Merka held a National Research Council Research Associateship Award at NASA/GSFC. Simulation results were provided by the Community Coordinated Modeling Center at NASA Goddard Space Flight Center through their public Runs on Request System. The CCMC is a multi-agency partnership between NASA, AFMC, AFOSR, AFRL, AFWA, NOAA, NSF, and ONR. The BATSRUS model was developed by the Center for Space Environment Modeling at the University of Michigan with funding support from NASA ESS, NASA ESTO-CT, NSF KDI, and DoD MURI.

[46] Shadia Rifai Habbal thanks Aleksey V. Dmitriev and Jacqueline Chapman for their assistance in evaluating this paper.

References

- Aubry, M. B., C. T. Russell, and M. G. Kivelson (1970), Inward motion of the magnetopause before a substorm, *J. Geophys. Res.*, *75*, 7018.
- Bennett, L., M. G. Kivelson, K. K. Khurana, L. A. Frank, and W. R. Paterson (1997), A model of the Earth's distant bow shock, *J. Geophys. Res.*, *102*, 26,927–26,941.
- Berkowitz, J., H. Grad, and H. Rubin (1958), Magnetohydrodynamic stability, in *Proceedings of the 2nd U. N. International Conference on Peaceful Uses of Atomic Energy*, vol. 31, p. 177, U. N., New York.
- Bieber, J. W., and E. C. Stone (1979), Energetic electron bursts in the magnetopause electron layer and in interplanetary space, in *Proceedings of Magnetospheric Boundary Layers Conf., ESA SP-148*, pp. 131–135, Eur. Space Agency, Paris.
- Binsack, J. H., and V. M. Vasyliunas (1968), Simultaneous IMP-2 and OGO-I observations of bow shock compression, *J. Geophys. Res.*, *73*, 429.
- Boardman, S. A., T. E. Eastman, T. Sotirelis, and J. L. Green (2000), An empirical model of the high-latitude magnetopause, *J. Geophys. Res.*, *105*, 23,193–23,219.
- Cairns, I. H., and C. L. Grabbe (1994), Towards an MHD theory for the standoff distance of Earth's bow shock, *Geophys. Res. Lett.*, *21*, 2781–2784.
- Cairns, I. H., and C. L. Grabbe (1996), Reply to comment on “Towards an MHD theory for the standoff distance of Earth's bow shock” by C. T. Russell and S. M. Petrinec, *Geophys. Res. Lett.*, *23*, 311–314.
- Cairns, I. H., and J. G. Lyon (1995), MHD simulations of Earth's bow shock at low Mach numbers: Standoff distances, *J. Geophys. Res.*, *100*, 17,173–17,180.
- Cairns, I. H., and J. G. Lyon (1996), Magnetic field orientation effects on the standoff distance of Earth's bow shock, *Geophys. Res. Lett.*, *23*, 2883–2886.
- Cairns, I. H., D. H. Fairfield, R. R. Anderson, V. E. H. Carlton, K. I. Paularena, and A. J. Lazarus (1995), Unusual locations of Earth's bow shock on September 24–25, 1987: Mach number effects, *J. Geophys. Res.*, *100*, 47–62.
- Chapman, J. F., and I. H. Cairns (2003), Three-dimensional modeling of Earth's bow shock: Shock shape as a function of Alfvén Mach number, *J. Geophys. Res.*, *108*(A8), 1179, doi:10.1029/2001JA000219.
- Chapman, J. F., I. H. Cairns, J. G. Lyon, and C. R. Boshuizen (2004), MHD simulations of Earth's bow shock: Interplanetary magnetic field orientation effects on shape and position, *J. Geophys. Res.*, *109*, A04215, doi:10.1029/2003JA010235.
- Chapman, S., and V. C. A. Ferraro (1931), A new theory of magnetic storm, I, The initial phase, *J. Geophys. Res.*, *36*, 77.
- De Sterck, H., and S. Poedts (1999), Field-aligned magnetohydrodynamic bow shock flows in the switch-on regime, *Astron. Astrophys.*, *343*, 641–649.

- De Sterck, H., B. C. Low, and S. Poedts (1998), Complex magnetohydrodynamic bow shock topology in field-aligned low- β flow around a perfectly conducting cylinder, *Phys. Plasmas*, *5*, 4015–4027.
- Dmitriev, A. V., and A. V. Suvorova (2000), Three-dimensional artificial neural network model of the dayside magnetopause, *J. Geophys. Res.*, *105*, 18,909–18,918.
- Dmitriev, A. V., J. K. Chao, and D.-J. Wu (2003), Comparative study of bow shock models using Wind and Geotail observations, *J. Geophys. Res.*, *108*(A12), 1464, doi:10.1029/2003JA010027.
- Efron, B. (1979), Bootstrap methods: Another look at the jackknife, *Ann. Stat.*, *7*, 1–26.
- Fairfield, D. H. (1971), Average and unusual locations of the Earth's magnetopause and bow shock, *J. Geophys. Res.*, *76*, 6700–6715.
- Fairfield, D. H., I. H. Cairns, M. D. Desch, A. Szabo, A. J. Lazarus, and M. R. Aellig (2001), The location of low Mach number bow shock at Earth, *J. Geophys. Res.*, *106*, 25,361–25,376.
- Farris, M. H., and C. T. Russell (1994), Determining the standoff distance of the bow shock: Mach number dependence and use of models, *J. Geophys. Res.*, *99*, 17,681–17,689.
- Farris, M. H., S. M. Petrinec, and C. T. Russell (1991), The thickness of the magnetosheath: Constraints on the polytropic index, *Geophys. Res. Lett.*, *18*, 1821–1824.
- Formisano, V. (1979), Orientation and shape of the Earth's bow shock in three dimensions, *Planet. Space Sci.*, *27*, 1151–1161.
- Formisano, V., V. Domingo, and K.-P. Wenzel (1979), The three-dimensional shape of the magnetopause, *Planet. Space Sci.*, *27*, 1137–1149.
- Grad, H., and P. Hu (1966), Neutral point in the geomagnetic field, *Phys. Fluids*, *9*, 1610.
- Holzer, R. E., and J. A. Slavin (1978), Magnetic flux transfer associated with expansions and contractions of the dayside magnetosphere, *J. Geophys. Res.*, *83*, 3831.
- Kabin, K. (2001), A note on the compression ratio in MHD shocks, *J. Plasma Phys.*, *66*, 259–274.
- Kawano, H., and T. Higuchi (1995), The bootstrap method in space physics: Error estimation for the minimum variance analysis, *Geophys. Res. Lett.*, *22*, 307–310.
- Kawano, H., S. M. Petrinec, C. T. Russell, and T. Higuchi (1999), Magnetopause shape determinations from measured position and estimated flaring angle, *J. Geophys. Res.*, *104*, 247.
- Kuznetsov, S. N., and A. V. Suvorova (1998), An empirical model of the magnetopause for broad ranges of solar wind pressure and b_2 IMF, in *Polar Cap Boundary Phenomena*, edited by J. M. et al., p. 51, Kluwer Acad., Norwell, Mass.
- Landau, L. D., and E. M. Lifshitz (1959), *Fluid Mechanics*, pp. 310–313, Pergamon, New York.
- Marquardt, D. W. (1963), An algorithm for least-squares estimation of nonlinear parameters, *J. Soc. Indust. Appl. Math.*, *11*, 431–441.
- Merka, J., A. Szabo, T. W. Narock, J. H. King, K. I. Paularena, and J. D. Richardson (2003a), A comparison of IMP 8 observed bow shock positions with model predictions, *J. Geophys. Res.*, *108*(A2), 1077, doi:10.1029/2002JA009384.
- Merka, J., A. Szabo, J. Šafránková, and Z. Němeček (2003b), Earth's bow shock and magnetopause in the case of a field-aligned upstream flow: Observation and model comparison, *J. Geophys. Res.*, *108*(A7), 1269, doi:10.1029/2002JA009697.
- Merka, J., A. Szabo, T. W. Narock, J. D. Richardson, and J. H. King (2004), Three decades of bow shock observations by IMP 8 and model predictions, *Planet. Space Sci.*, in press.
- Michel, F. C. (1965), Detectability of disturbances in the solar wind, *J. Geophys. Res.*, *70*, 1.
- Němeček, Z., J. Měrka, and J. Šafránková (2000), The tilt angle control of the outer cusp position, *Geophys. Res. Lett.*, *27*, 77–80.
- Peredo, M., D. P. Stern, and N. A. Tsyganenko (1993), Are existing magnetospheric models excessively stretched?, *J. Geophys. Res.*, *98*, 15,343–15,354.
- Peredo, M., J. A. Slavin, E. Mazur, and S. A. Curtis (1995), Three-dimensional position and shape of the bow shock and their variation with Alfvénic, sonic and magnetosonic Mach numbers and interplanetary magnetic field orientation, *J. Geophys. Res.*, *100*, 7907–7916.
- Petrinec, S. M., and C. T. Russell (1993), An empirical model of the size and shape of the near-Earth magnetotail, *Geophys. Res. Lett.*, *20*, 2695.
- Petrinec, S. M., and C. T. Russell (1995), An examination of the effect of dipole tilt angle and cusp regions on the shape of the dayside magnetopause, *J. Geophys. Res.*, *100*, 9559–9566.
- Petrinec, S. M., and C. T. Russell (1996), Near-Earth magnetotail shape and size as determined from the magnetopause flaring angle, *J. Geophys. Res.*, *101*, 137–152.
- Petrinec, S. M., and C. T. Russell (1997), Hydrodynamic and MHD equations across the bow shock and along the surfaces of planetary obstacles, *Space Sci. Rev.*, *79*, 757–791.
- Petrinec, S. M., P. Song, and C. T. Russell (1991), Solar cycle variations in the size and shape of the magnetopause, *J. Geophys. Res.*, *96*, 7893–7896.
- Roelof, E. C., and D. G. Sibeck (1993), Magnetopause shape as a bivariate function of interplanetary magnetic field b_2 and solar wind dynamic pressure, *J. Geophys. Res.*, *98*, 21,421.
- Russell, C. T., and S. M. Petrinec (1996), Comments on “Towards an MHD theory for the standoff distance of Earth's bow shock” by I. H. Cairns and C. L. Grabbe, *Geophys. Res. Lett.*, *23*, 309–310.
- Russell, C. T., and T. L. Zhang (1992), Unusually distant bow shock encounters at Venus, *Geophys. Res. Lett.*, *19*, 833–836.
- Šafránková, J., Z. Němeček, S. Dušák, L. Přeč, D. G. Sibeck, and N. N. Borodkova (2002), The magnetopause shape and location: A comparison of the Interball and Geotail observations with models, *Ann. Geophys.*, *20*, 301–309.
- Shue, J.-H., J. K. Chao, H. C. Fu, C. T. Russell, P. Song, K. K. Khurana, and H. J. Singer (1997), A new functional form to study the solar wind control of the magnetopause and shape, *J. Geophys. Res.*, *102*, 9497–9511.
- Shue, J.-H., et al. (1998), Magnetopause location under extreme solar wind conditions, *J. Geophys. Res.*, *103*, 17,691–17,700.
- Sibeck, D. G., R. E. Lopez, and E. C. Roelof (1991), Solar wind control of the magnetopause shape, location, and motion, *J. Geophys. Res.*, *96*, 5489–5495.
- Slavin, J. A., and R. E. Holzer (1981), Solar wind flow about the terrestrial planets, 1, Modeling bow shock position and shape, *J. Geophys. Res.*, *86*, 11,401–11,418.
- Slavin, J. A., R. E. Holzer, J. R. Spreiter, and S. S. Stahara (1984), Planetary Mach cones: Theory and observation, *J. Geophys. Res.*, *89*, 2708–2714.
- Slavin, J. A., A. Szabo, M. Peredo, C. J. Owen, R. P. Lepping, R. Fitzenreiter, R. W. Ogilvie, J. L. Stremberg, and A. J. Lazarus (1996), Near-simultaneous bow shock crossings by Wind and IMP 8 on December 1, 1994, *Geophys. Res. Lett.*, *23*, 1207–1210.
- Spreiter, J. R., and B. R. Briggs (1962), Theoretical determination of the form of the boundary of the solar corpuscular stream produced by interaction with the magnetic dipole field of the earth, *J. Geophys. Res.*, *67*, 37–51.
- Spreiter, J. R., and A. W. Rizzi (1974), Aligned MHD solution for solar wind flow past the Earth's magnetosphere, *Acta Astronaut.*, *1*, 15–35.
- Spreiter, J. R., and S. S. Stahara (1985), Magnetohydrodynamic and gas-dynamic theories for planetary bow waves, in *Collisionless Shocks in the Heliosphere: Reviews of Current Research*, *Geophys. Monogr. Ser.*, vol. 35, edited by B. T. Tsurutani and R. G. Stone, pp. 85–107, AGU, Washington, D. C.
- Spreiter, J. R., A. L. Summers, and A. Y. Alksne (1966), Hydromagnetic flow around the magnetosphere, *Planet. Space Sci.*, *14*, 223–253.
- Tsyganenko, N. A. (1989), A magnetospheric magnetic field model with a warped tail current sheet, *Planet. Space Sci.*, *37*, 1037–1046.
- Tsyganenko, N. A. (2002a), A model of the near magnetosphere with a dawn-dusk asymmetry, 1. Mathematical structure, *J. Geophys. Res.*, *107*(A8), 1179, doi:10.1029/2001JA000219.
- Tsyganenko, N. A. (2002b), A model of the near magnetosphere with a dawn-dusk asymmetry, 2. Parameterization and fitting to observations, *J. Geophys. Res.*, *107*(A8), 1176, doi:10.1029/2001JA000220.
- Verigin, M., G. Kotova, A. Szabo, J. Slavin, T. Gombosi, K. Kabin, F. Shugaev, and A. Kalinchenko (2001), WIND observations of the terrestrial bow shock: 3-D shape and motion, *Earth Planets Space*, *53*, 1001–1009.
- Verigin, M., J. A. Slavin, A. Szabo, G. Kotova, and T. Gombosi (2003), Planetary bow shocks: Asymptotic MHD Mach cones, *Earth Planets Space*, *55*, 33–38.
- Wu, C. C. (1984), The effects of dipole tilt on the structure of the magnetosphere, *J. Geophys. Res.*, *89*, 11,048–11,052.
- Zhou, X.-W., and C. T. Russell (1997), The location of the high-latitude polar cusp and the shape of the surrounding magnetopause, *J. Geophys. Res.*, *102*, 105–110.
- Zhou, X.-W., C. T. Russell, G. Le, S. A. Fuselier, and J. D. Scudder (1999), The Polar cusp location and its dependence on dipole tilt, *Geophys. Res. Lett.*, *26*, 429.

J. Merka and A. Szabo, Laboratory for Extraterrestrial Physics, NASA Goddard Space Flight Center, Code 696, Greenbelt, MD 20771, USA. (jan.merka@gssc.nasa.gov; adam.szabo@gssc.nasa.gov)